SPH simulation of solitary wave interaction with a curtain-type breakwater

Simulation par la méthode SPH de l'interaction d'une onde solitaire avec un brise-lames de type rideau

SONGDONG SHAO, Formerly JSPS Postdoctoral Fellow, *Coastal and Offshore Engineering, Department of Civil Engineering, Kyoto University, Kyoto 606-8501, Japan. E-mail: shao@coast.kuciv.kyoto-u.ac.jp* (Currently Research Fellow, *School of Mathematics and Statistics, University of Plymouth, Drake Circus, Plymouth, PL4 8AA, UK. Tel.: +441752232791; fax: +441752232780; E-mail: songdong.shao@plymouth.ac.uk*)

ABSTRACT

An incompressible Smoothed Particle Hydrodynamics (SPH) method is put forward to simulate non-linear and dispersive solitary wave reflection and transmission characteristics after interacting with a partially immersed curtain-type breakwater. The Naviers–Stokes equations in Lagrangian form are solved using a two-step split method. The method first integrates the velocity field in time without enforcing incompressibility. Then the resulting deviation of particle density is projected into a divergence-free space to satisfy incompressibility by solving a pressure Poisson equation. Basic SPH formulations are employed for the discretization of relevant gradient and divergence operators in the governing equations. The curtain wall and horizontal bottom are also numerically treated by fixed wall particles and the free surface of wave is tracked by particles with a lower density as compared with inner particles. The proposed SPH model is first verified by the test of a solitary wave with different amplitudes running against a vertical wall without opening underneath. Then it is applied to simulate solitary wave interacting with a partially immersed curtain wall with different immersion depths. The characteristics of wave reflection, transmission, dissipation and impacting forces on the curtain breakwater are discussed based on computational results.

RÉSUMÉ

La méthode Smoothed Particle Hydrodynamics (SPH) est proposée pour simuler les caractéristiques de la réflexion et de la transmission d'une onde solitaire non linéaire et dispersive après avoir interagi avec un brise-lames de type rideau partiellement immergé. Les équations de Navier-Stokes sous forme lagrangienne sont résolues en utilisant la méthode des pas fractionnaires en deux étapes. La méthode intègre d'abord le champ de vitesses dans le temps sans condition d'incompressibilité. Puis la variation résultante de la densité des particules est projetée dans un espace à divergence-libre pour satisfaire la condition d'incompressibilité en résolvant une équation de Poisson pour la pression. Les formulations de base de SPH sont utilisées pour la discrétisation des opérateurs appropriés de gradient et de divergence dans les équations. Le mur de rideau et le fond horizontal sont traités numériquement par des particules fixes de mur et la surface libre de la vague est suivie par des particules de densité plus faible que les particules intérieures. Le modèle proposé SPH est d'abord testé dans le cas d'une onde solitaire avec différentes amplitudes fonctionnant contre un mur vertical sans ouverture inférieure. Ensuite il est appliqué à la simulation d'une onde solitaire agissant sur un rideau partiellement immergé à différentes profondeurs. La réflexion, la transmission, la dissipation et les efforts sur le brise-lames sont présentés sur la base des résultats de calcul.

Keywords: Smoothed Particle Hydrodynamics, solitary wave, curtain-type breakwater.

1 Introduction

Upon reaching the shoreline, tsunamis can break and travel inland for large distances with potential damages for coastal environment, human property and life. Thus dissipation of wave height and energy from propagating waves is of basic necessity in coastal engineering. Different types of wave breakwaters have been designed throughout the world for this purpose. Among them the fixed-type breakwater, such as rubble mound breakwaters of the gravity type, is widely used due to its stability and easy construction. However, the cost of such breakwater will increase extremely with the increasing water depth. Besides, sometimes it is harmful to coastal environment since it almost cuts off the normal interrelationship between offshore and near-shore regions.

A curtain-type breakwater, being a rigid impermeable vertical wall ascending from a fraction of the water depth upwards, has many advantages. Different from the conventional gravity-type breakwater, it is less dependent on the geo-technical conditions of the sea bottom on which it is to be installed and thus its cost is relatively low. Besides, tsunamis can often be simplified as solitary wave or combinations of negative and positive solitary-like waves. The barrier can effectively intercept these kinds of long waves, whose energy is mostly concentrated within near the surface. At the same time, water circulation is maintained in the gap below, and the flow of sediment and maritime life near the seabed
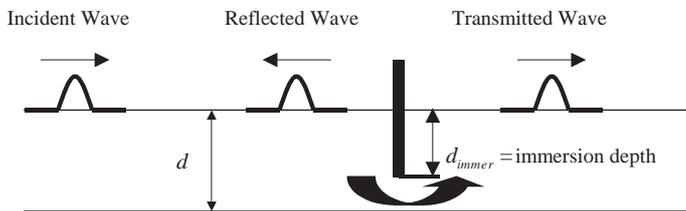
Figure 1   Sketch view of curtain breakwater for tsunami control.

is unimpeded. In practice, the curtain barrier can be supported on piles driven along the breakwater alignment for rigidity. The partially immersed curtain breakwater for tsunami control can be conceptually described in Fig. 1, where the immersion index d_{immer}/d is defined by the ration of d_{immer} (which is the distance between the water surface and the bottom tip of the curtain wall) over local water depth d.

This old issue had been earlier addressed by Ursell (1947), who derived an analytical solution for the partial transmission and reflection of deep water waves interacting with a fixed vertical infinitely thin barrier, extending from the water surface to some depth below this surface. Wiegel (1960) developed a theory based on power transmission for the same problem and obtained valuable experimental data to verify his theory. Later Reddy and Neelamani (1992) expanded this theory and carried out a detailed experimental investigation to determine the characteristics of wave reflection and transmission by a curtain wall for a wide range of wave steepness and different immersion depths of the barrier. Investigations have also been extended to the configuration of the curtain wall to include vertical slotted or slit-type wave barriers (Kriebel *et al.*, 1998), porous screens (Losada *et al.*, 1993) and multiple permeable barriers (Lee and Lee, 2001; Neelamani and Vedagiri, 2002), in which the wave energy dissipation occurs within the barriers. A relevant review has been made by Lo (2000), who also carried out a detailed study on the issue of flexible curtain-type wave barriers consisting of vertically tensioned membrane by using an eigenfunction approach. However, the solitary wave application has been paid little attention in the above-mentioned literatures. One of the main reasons might be that either the theoretical or experimental techniques they employed were not able to deal appropriately with the problems of large amplitude wave characterized by strong non-linearity and dispersion such as in the case of a solitary wave.

Numerical models based on the solutions of the Navier–Stokes (N–S) equation have become increasingly popular to address this problem up to, and even beyond wave breaking, since they can provide full details of the flow in the region of interest. The philosophy of the Smoothed Particle Hydrodynamics (SPH) method is employed in the paper as the N–S solver. SPH first originated in astrophysics for the study of dynamics of interstellar gas (Lucy, 1977) and also provided a powerful tool to model a wide range of hydrodynamics problems. The basic concept of the SPH is that any field variable of a reference particle can be expressed with enough accuracy by integrals, which are approximated by summation interpolants over neighboring particles. From this point, spatial derivatives such as the gradient and divergence operators in the N–S equation can be similarly evaluated by summation

interpolants with particle properties. One of the great advantages of the SPH modeling of free surface flows is that particles move in Lagrangian coordinates and advection is directly calculated by particle motion. Thus free surface can be conveniently and accurately tracked by particles without numerical diffusion, which is usually encountered in the traditional Eulerian approach. In early simulations of fluid flows by SPH, incompressibility is realized through an equation of state so that the fluid is assumed to be slightly compressible (Monaghan and Kos, 1999). In this case, a large sound speed has to be introduced, which could easily cause problems of sound wave reflection at the boundary and the high sound speed leads to a crippling CFL time-step constraint (Cummins and Rudman, 1999). Here a real incompressible SPH conception is proposed similar to that of the SPH projection employed by Cummins and Rudman (1999). The pressure is not a thermodynamic variable obtained from the equation of state, but obtained by way of solving a pressure Poisson equation derived from a semi-implicit algorithm. The simulations of a vortex spin-down and Rayleigh–Taylor instability by Cummins and Rudman (1999) showed that both the computational efficiency and stability have been improved as compared with the initial weakly compressible SPH numerical schemes.

The paper is organized in the following ways. First, the numerical SPH model is introduced including governing equations and various SPH formulations. Then the proposed model is validated by the test of a solitary wave with different amplitudes running against a vertical wall without opening underneath. Finally it is applied to simulate solitary wave interacting with a partially immersed curtain wall with different immersion depths. The characteristics of wave reflection, transmission, dissipation and impacting forces on the curtain breakwater are discussed based on computational results. The study in the paper provides basic information for understanding the efficiencies of this type of special breakwater. The findings on the characteristics of wave transmission are essential to select the appropriate configuration of such breakwater for a prevailing wave climate once the permissible range of transmission has been decided for the harbor side operations.

2   Governing equation and equation solver

The SPH model solves the N–S equations in Lagrangian form

$$\frac{1}{\rho}\frac{D\rho}{Dt} + \nabla \cdot \mathbf{u} = 0 \tag{1}$$

$$\frac{D\mathbf{u}}{Dt} = -\frac{1}{\rho}\nabla P + \mathbf{g} + \nu_0\nabla^2\mathbf{u} \tag{2}$$

where ρ = fluid particle density; t = time; $\mathbf{u}$ = particle velocity; P = particle pressure; $\mathbf{g}$ = gravitational acceleration and $\nu_0 = \mu_0/\rho$ = laminar kinematic viscosity. It is noted that Eq. (1) is represented in the form of a compressible flow. Incompressibility is enforced by way of setting $D\rho/Dt = 0$ at each particle during the computation.

The prediction–correction scheme of the incompressible SPH method consists of two steps similar to the two-step projection

method of Chorin (1968) for solving the N–S equations. The prediction step is an explicit integration in time without enforcing incompressibility. Only the laminar viscous and gravitational terms in the N–S Eq. (2) are used and an intermediate particle velocity and position are obtained

$$\Delta \mathbf{u}_* = (\mathbf{g} + \nu_0 \nabla^2 \mathbf{u}) \Delta t \tag{3}$$

$$\mathbf{u}_* = \mathbf{u}_t + \Delta \mathbf{u}_* \tag{4}$$

$$\mathbf{r}_* = \mathbf{r}_t + \mathbf{u}_* \Delta t \tag{5}$$

where $\Delta \mathbf{u}_* =$ changed particle velocity during the prediction step; $\Delta t =$ time increment; $\mathbf{u}_t$ and $\mathbf{r}_t =$ particle velocity and position at time t; and $\mathbf{u}_*$ and $\mathbf{r}_* =$ intermediate particle velocity and position.

Then the second correction step is applied to adjust fluid densities at the particles to initial values prior to the prediction step. In the correction, the pressure term is used to update the particle velocity obtained from the intermediate step. The relevant procedures are

$$\Delta \mathbf{u}_{**} = -\frac{1}{\rho_*} \nabla P_{t+1} \Delta t \tag{6}$$

$$\mathbf{u}_{t+1} = \mathbf{u}_* + \Delta \mathbf{u}_{**} \tag{7}$$

where $\Delta \mathbf{u}_{**} =$ changed particle velocity during the correction step; $\rho_* =$ intermediate particle density between the prediction and correction; and P_{t+1} and $\mathbf{u}_{t+1} =$ particle pressure and velocity of time $t + 1$.

Finally the positions of particle are centered in time

$$\mathbf{r}_{t+1} = \mathbf{r}_t + \frac{(\mathbf{u}_t + \mathbf{u}_{t+1})}{2} \Delta t \tag{8}$$

where $\mathbf{r}_t$ and $\mathbf{r}_{t+1} =$ positions of particle in time t and $t + 1$.

The pressure for enforcing incompressibility in the correction step is obtained from the mass conservation Eq. (1) represented in the discrete form by SPH particles as

$$\frac{1}{\rho_0} \frac{\rho_0 - \rho_*}{\Delta t} + \nabla \cdot (\Delta \mathbf{u}_{**}) = 0 \tag{9}$$

where $\rho_0 =$ initial constant density at each of the particles.

Combining Eqs (6) and (9), the pressure Poisson equation is obtained as follows

$$\nabla \cdot \left(\frac{1}{\rho_*} \nabla P_{t+1} \right) = \frac{\rho_0 - \rho_*}{\rho_0 \Delta t^2} \tag{10}$$

The above equation solver is also analogous to that employed in the Moving Particle Semi-implicit (MPS) method (Koshizuka *et al.*, 1998; Gotoh and Sakai, 1999) in that the source term of the Poisson equation is the variation of particle densities, while it is usually the divergence of intermediate velocity in finite difference methods. By employing the relevant SPH formulations in the following section, Eq. (10) is discretized into simultaneous linear equations whose matrix is symmetric and positive definite. These equations can be solved efficiently by using the Incomplete Cholesky Conjugate Gradient (ICCG) method (Hirsch, 1990). By using this semi-implicit algorithm, the stability of pressure due to the change of particle density is well improved and the stable pressures have been obtained in a dam-break simulation by Shao

and Lo (2003). Convergence of the iteration is assumed to be satisfactory when the difference between two successive iteration steps reduces to 0.1 Pa and approximately two to six iterations are required for the pressure equation. The incompressible SPH scheme was found to be first-order accurate globally (Shao and Lo, 2003).

3   SPH formulations

The SPH formulations as developed by Monaghan (1992) are obtained by interpolating from a set of points that may be disordered. The interpolation is based on the theory of integral interpolants using kernels that approximate a delta function. The interpolants are analytic functions that can be differentiated exactly. If the points are fixed in position, the equations reduce to finite difference equations, with different forms depending on the interpolation kernel. The SPH equations describe the motion of the interpolating points, which can be thought of as particles. Each particle carries a mass m, a velocity $\mathbf{u}$, and other properties, depending on the problem.

Using the above concepts, any quantity of particle a, whether scalar or vector, can be approximated by the direct summation of the relevant quantities of its neighboring particles b

$$\varphi_a(\mathbf{r}_a) = \sum_b m_b \frac{\varphi_b(\mathbf{r}_b)}{\rho_b(\mathbf{r}_b)} W(|\mathbf{r}_a - \mathbf{r}_b|, h) \tag{11}$$

where a and $b =$ reference particle and its neighbors; φ_a and $\varphi_b =$ scalar or vector quantity being interpolated and interpolating; $\mathbf{r}_a$ and $\mathbf{r}_b =$ position of particles; and $W =$ interpolation kernel and $h =$ smoothing distance. Thus the fluid density at particle a, ρ_a is evaluated by

$$\rho_a = \sum_b m_b W(|\mathbf{r}_a - \mathbf{r}_b|, h) \tag{12}$$

Kernels can assume many different forms and the use of different kernels is the SPH analog of using different difference schemes in finite difference methods. By balancing the computational accuracy and efficiency, the following kernel based on the spline function and normalized in two dimensional (2-D) is adopted (Monaghan, 1992)

$$
\begin{aligned}
W(r, h) &= \frac{10}{7\pi h^2} \left(1 - \frac{3}{2} q^2 + \frac{3}{4} q^3 \right) && q < 1 \\
W(r, h) &= \frac{10}{28\pi h^2} (2 - q)^3 && 1 \leq q \leq 2 \\
W(r, h) &= 0 && q > 2
\end{aligned}
\tag{13}
$$

where $q = r/h$ and $r =$ separation distance between the particles. The smoothing distance or kernel range h determines the degree by which a particle interacts with neighboring particles. In the subsequent computation h is set twice the initial particle spacing.

The gradient term has different forms depending on the derivation used. The following symmetric form is widely used since it

conserves linear and angular momentum exactly. For example, the gradient of the pressure is expressed as

$$\left(\frac{1}{\rho}\nabla P\right)_a = \sum_b m_b \left(\frac{P_a}{\rho_a^2} + \frac{P_b}{\rho_b^2}\right) \nabla_a W_{ab} \tag{14}$$

where the summation is over all particles other than particle a and $\nabla_a W_{ab}$ = gradient of the kernel taken with respect to the positions of particle a. Similarly, the divergence of a vector $\mathbf{u}$ at particle a can be formulated symmetrically by

$$\nabla \cdot \mathbf{u}_a = \rho_a \sum_b m_b \left(\frac{\mathbf{u}_a}{\rho_a^2} + \frac{\mathbf{u}_b}{\rho_b^2}\right) \cdot \nabla_a W_{ab} \tag{15}$$

In order to avoid pressure instability and decoupling in the computation, the Laplacian is formulated as a hybrid of a standard SPH first derivative with a finite difference approximation for the first derivative, which is similar to the approach by Cummins and Rudman (1999)

$$\nabla \cdot \left(\frac{1}{\rho}\nabla P\right)_a = \sum_b m_b \frac{8}{(\rho_a + \rho_b)^2} \frac{P_{ab}\mathbf{r}_{ab} \cdot \nabla_a W_{ab}}{|\mathbf{r}_{ab}|^2} \tag{16}$$

where $P_{ab} = P_a - P_b$ and $\mathbf{r}_{ab} = \mathbf{r}_a - \mathbf{r}_b$ are defined.

Using the same rule the SPH formulation of the laminar viscous term in Eq. (2) is

$$(\nu_0 \nabla^2 \mathbf{u})_a = \sum_b \frac{4m_b(\mu_a + \mu_b)\mathbf{r}_{ab} \cdot \nabla_a W_{ab}}{(\rho_a + \rho_b)^2(|\mathbf{r}_{ab}|^2)}(\mathbf{u}_a - \mathbf{u}_b) \tag{17}$$

The above equation is based on a similar SPH expression used by Monaghan (1992) to model heat conduction. The expression conserves linear momentum exactly, while angular momentum is only approximately conserved.

4 Numerical treatment of solid walls and free surface

4.1 Wall boundaries

The solid walls are also simulated by particles, which balance the pressure of inner fluid particles and prevent them from penetrating the wall. Here we follow the treatment used by Koshizuka *et al.* (1998) and Gotoh and Sakai (1999) to model the wall boundaries such as the partially immersed curtain wall by fixed wall particles, which are equally spaced according to the geometric configurations of the wall. The pressure Poisson Eq. (10) is solved on these wall particles to repulse the inner flow particles accumulating in the vicinity of the wall. For example, the pressure of wall particles increases when the particle density in the vicinity of the wall increases and thus the inner fluid particles are repelled away from the wall, and vice versa. The velocities of wall particles are set to be zero to represent the no-slip boundary conditions. In order to impose the homogeneous Neumann boundary condition on wall particles, several lines of dummy particles are put on the other side of the wall and the pressure of these dummy particles is set to be equal to the pressure of neighboring wall particles. Thus the normal pressure gradient of wall particles is approximately zero and we only consider the interactions between neighboring wall particles and inner fluid particles while solving the pressure equation.

4.2 Free surfaces

Free surfaces are easily identified by particle densities. Since no particle exists in the outer region of the free surface, the particle density will drop suddenly on the surface. A particle is regarded as a surface particle if the absolute value of the difference between the particle density and reference density exceeds $0.01\rho_0$. A Dirichlet boundary condition of zero pressure is given to this particle. Unlike wall particles, surface particles are not considered in the pressure Poisson equation.

5 Computational efficiency

In the incompressible SPH method, each fluid particle needs a list of neighboring particles within a distance of kernel range ($2h$ in this paper). The whole list, which is updated in each time step, requires the scale of N^2 operations for the calculation of distances between all pairs of particles, where N is the number of particles. This list generation can dominate the computation time in large problems involving many particles.

In order to improve computational efficiency, linked list data structures put forward by Monaghan and Lattanzio (1985) are employed to identify neighboring particles within a distance of $2h$. The computational domain is divided into square cells having side lengths of $2h$ and a list of particles belonging to each cell is created. A particle located within a given cell then considers interactions only with particles in neighboring cells. In this way, computational efficiency is significantly improved.

In addition, the time step is also dynamically adjusted in the computation for acceleration based on the following Courant condition

$$\Delta t \le 0.1 \frac{l_0}{V_{\max}} \tag{18}$$

and the constraint of viscous diffusion

$$\Delta t \le 0.1 \frac{l_0^2}{\nu_0} \tag{19}$$

where $V_{\max}$ = maximum particle velocity and l_0 = typical particle spacing.

6 Model verification

In this section the proposed incompressible SPH model is validated by the non-linear reflection of high amplitude solitary waves from a vertical wall. When low amplitude solitary waves collide with a vertical wall, they behave as solitons and reflect without reduction in the wave height and speed. However, in case of highly non-linear solitary waves with large amplitude, the reflected wave will lose part of the energy to a dispersive tail. Thus the height and speed of the reflected wave are smaller than those of the incident wave before collision. This problem has been addressed extensively in the literatures, represented by Cooker *et al.* (1997) using a boundary-integral method for solving the Eulerian equations and by Madsen *et al.* (2002) using a high-order Boussinesq approximation with fully non-linear boundary

conditions. Their numerical results are employed here to test the SPH model.

Generally speaking, the following sequences of events occur during the whole impact processes of the solitary wave. Initially the incident wave propagates with constant speed and wave height. As the wave crest is less than about twice the water depth from the wall, the wave crest accelerates significantly. At the instant time t_a (the so-called attachment time in Cooker *et al.*, 1997), the wave crest snaps through to the wall with a corresponding elevation η_a. With a little delay up to time t_0, the maximum run-up occurs with an elevation η_0, which can be several times larger than the incident amplitude. After a further delay, the wave crest leaves the wall at t_d (the so-called detachment time) with an elevation η_d, which is always less than η_a. It follows that $t_0 - t_a < t_d - t_0$, i.e., the time of water line falling is always longer than the time of rising. Besides, the total time during which the crest is attached to the wall is called the wall residence time defined by $t_r = t_d - t_a$, which provides an unambiguous characterization of the phase shift incurred during reflection for waves of both small and large amplitudes. For small and moderate amplitude solitary waves there will be very little difference in wave height and speed as compared with the perfect reflection soliton behavior. As for high amplitude solitary waves with strong non-linearity and dispersion, the behavior is totally different.

In the following analysis, $\tau = (d/\mathbf{g})^{1/2}$ is the dimensional time scale and $\varepsilon = a/d$ is the dimensionless wave amplitude, a being the amplitude of the incident wave traveling on a fluid with a constant water depth d. A series of SPH simulations have been made with non-linearity parameter ε ranging from 0.05 to 0.75. We consider a constant water depth of 1.0 m and computational domain 40.0 m long, which is long enough to eliminate the influence of the vertical wall on the initialization of the solitary wave profile at the beginning of the computation. The initial condition is based on the solitary wave data of Tanaka (1986), whose numerical solution is extremely accurate even for the highest waves. The SPH particles are initially put on a Cartesian grid with a spacing of $l_0 = 5.0$ cm and thus about 16,000 particles are involved in the computation. The choice of the particle spacing l_0 is made balancing both the computational efficiency and accuracy. Generally speaking, the particle number in the vertical direction must be at least 20 in order to eliminate the effect of the bottom wall in a vertical 2-D case. Here it should be noted that the small wave amplitude ($\varepsilon = 0.05$) is of the same order as particle spacing l_0, which could strongly reduce the accuracy of SPH simulation in this case. The initial solitary wave is put on the entrance side of the computational domain, with each particle assuming a velocity and elevation as given by Tanaka (1986). This initialization of data for particles is similar to Monaghan and Kos (1999), who used solutions derived from Boussinesq equation. The horizontal distance from the wave crest to the wall is x_0, which for each wave is chosen so that the fluid elevation at the wall is always less than $10^{-5}d$ at the beginning of the simulation. This setting is also consistent with that used by Cooker *et al.* (1997) in a similar calculation. The computational time step Δt is automatically adjusted in the whole simulations required by the Courant constraint and viscous diffusion.

According to SPH computations, the normalized attachment elevation η_a, detachment elevation η_d and maximum run-up η_0, are plotted against the dimensionless incident wave amplitude ε in Fig. 2. The normalized instantaneous wall force as a function of time relative to t_0 (which is the time at maximum run-up) for selected values of ε, are shown in Fig. 3. The wall forces are obtained by integrating the pressure distributions over the wall from the seabed to the free surface. The pressure distribution is calculated integrating individual particle pressures and mapping them onto a 1.0 cm × 1.0 cm grid system inserted in the simulation domain. In both figures, the numerical results by Cooker *et al.* (1997) using a boundary-integral method to solve Euler equation with fully non-linear boundary conditions and by Madsen *et al.* (2002) using a high order Boussinesq approach to solve Laplace equation, are also shown for comparison. The good agreement
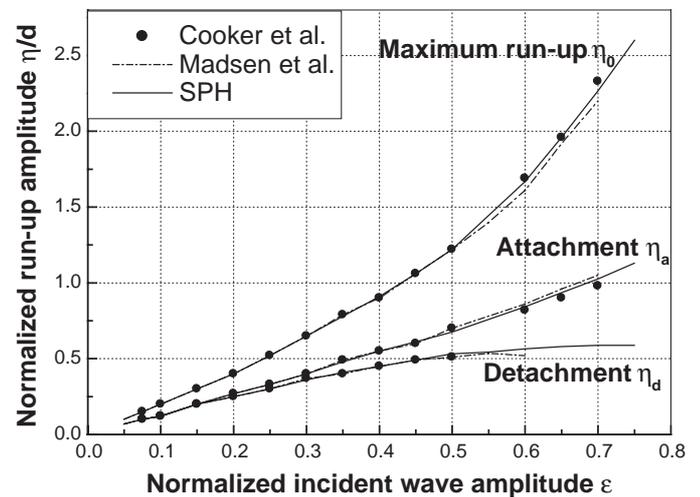

Figure 2 Normalized maximum run-up, attachment amplitude and detachment amplitude versus incoming wave amplitudes ε. Compared with numerical data of solitary wave reflecting from a vertical wall without opening underneath by Cooker *et al.* (1997) and Madsen *et al.* (2002).
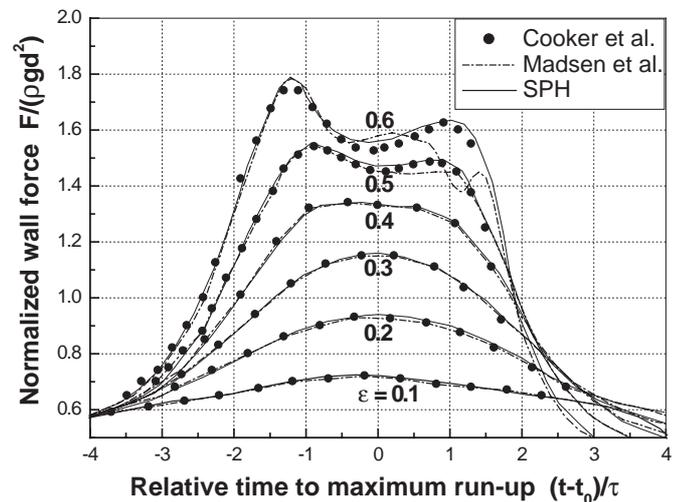

Figure 3 Normalized wall force versus time relative to maximum run-up t_0 for different incoming wave amplitudes ε. Compared with numerical data of solitary wave reflecting from a vertical wall without opening underneath by Cooker *et al.* (1997) and Madsen *et al.* (2002).

between them is quite satisfactory. However, both Cooker *et al.* (1997) and Madsen *et al.* (2002) reported a numerical breakdown in their computations when the non-linearity parameter ε exceeds 0.7. On the other hand, the SPH simulations are very stable even if ε reaches 0.75. One reason is that the advection term in the N–S equation is calculated by particles and the free surface is also tracked by particles without numerical diffusion in the SPH formulation. Thus it is capable of handling violent wave flows with large deformation during their run-up and rundown processes. Besides, it is also noted from Fig. 3 that the result of Madsen *et al.* (2002) deviates significantly from that of Cooker *et al.* (1997) at $\varepsilon = 0.6$. By comparison, the SPH result is quite consistent with that of Cooker *et al.* (1997), in which the curve follows a two-peak pattern rather than a three-peak one as reported by Madsen *et al.* (2002).

From Fig. 2 it is shown that the maximum run-up η_0 for weakly non-linear waves is approximately a linear function and more than twice the incident wave amplitude. At sufficiently high amplitude, i.e. $\varepsilon > 0.65$, the run-up increases non-linearly with ε and exceeds three times the incident wave amplitude. Besides, the attachment elevation η_a is always higher than the detachment elevation $\eta_d \cdot \eta_a$ increases almost linearly within the whole range of ε but with a much slower rate as compared with the maximum run-up. On the other hand, η_d increases only slightly with ε and seems to approach an asymptotic value at large ε, whose physical mechanism is yet to be adequately disclosed. Fig. 3 shows that for ε up to 0.3, the wall force is single peaked while it becomes double peaked for higher waves. This is attributed to the mutual interactions between the hydrostatic and dynamic pressures during the wave run-up and run-down processes. For small waves, the force is dominated by hydrostatic pressure and has a single maximum, which occurs around the time of maximum run-up at t_0. For waves with larger values of ε, the vertical acceleration of flow becomes more important, especially during the initial run-up stage. Thus it increases the pressure above the hydrostatic value and the first maximum occurs before the maximum run-up. During the maximum run-up, the acceleration forces are counteracting the hydrostatic forces, leading to a local minimum. Later at the end of wave run-down, the deceleration again increases the pressure above the hydrostatic value and creates a second peak in the force. However, its magnitude is slightly smaller as compared with the previous one.

7 Solitary wave reflection and transmission by partially immersed curtain breakwater

In this section, the solitary wave transmission and reflection by a partially immersed curtain breakwater are studied based on the above incompressible SPH model. The following computational parameters are employed. The initial water depth is $d = 20.0$ cm and the computational domain is 10.0 m long. The initial particle spacing is $l_0 = 1.0$ cm and totally 20,000 particles are used in the computation. Here the particle spacing l_0 assumes a smaller value as compared with that employed in the previous section. The purpose is to further improve the spatial accuracy. Meanwhile,

in order to reduce the computational cost, the constant water depth also assumes a smaller value. In this regard, the vertical scale of the simulation might deviate somewhat from the real situation. Nonetheless, this vertical scale is quite close to what is commonly used in most wave flume experiments and still has a practical meaning. The curtain wall is located at a distance of 4.0 m from the left boundary and the incident wave amplitude is chosen as $\varepsilon = a/d = 0.3$ and 0.6, respectively, in the simulation.

In order to evaluate the influence of different immersion conditions, four immersion depths of the curtain wall are selected, i.e., the immersion index is $d_{immer}/d = 0.0$, 0.25, 0.50 and 0.75. The curtain wall is assumed to be vertical, rigid and impermeable and overtopping is not considered here. The time step Δt is dynamically adjusted in the computation to satisfy the stability requirement of Eqs (18) and (19) and the kinematic viscosity is taken as $\nu_0 = 10^{-6}$ m²/s. The initial wave condition is described by giving the SPH particles near the entrance of the computational domain with a specified wave profile and velocity, based on the numerical solutions of Tanaka (1986).

7.1 Smaller amplitude solitary wave ($\varepsilon = 0.3$) impacting on curtain wall with different immersion depths

The reflection and transmission characteristics of a smaller amplitude solitary wave ($\varepsilon = 0.3$) are analyzed here using the SPH model. The time sequences of particle configurations of the solitary wave before and after interaction with the curtain wall are shown in Fig. 4(a–d) under the condition of $d_{immer}/d = 0.50$. In Fig. 4(a)–(d) corresponds to the incident wave, maximum runup, rundown and reflected and transmitted waves, respectively.

From the computation it is shown that after the incident wave impacts on the curtain wall, a transmitted wave is created due to the pressure difference on both sides of the wall. The redundant pressure on the left side pushes part of the water on the right to move in the form of a wave. This transmitted wave gradually develops into a stable solitary wave as it propagates further downstream. Meanwhile, the reflected waves are created by the interaction between the incident wave and the curtain wall. However, the reflection is not very clear and assumably composed of two parts. One part, which is far away from the curtain wall, was created by the direct reflection when the incident solitary wave approached the wall prior to its run-up. In contrast, another part, which is close to the curtain wall, was created by the rundown motion of the flow.

In order to quantitatively verify the accuracy of the above computations, the surface profiles of fully transmitted waves are shown in Fig. 5(a–d), under conditions of different immersion depths of $d_{immer}/d = 0.0$, 0.25, 0.50 and 0.75, respectively. Meanwhile the theoretical wave profiles based on the Boussinesq equation (Dean and Dalrymple, 1991) are given for comparison. The good agreement between the two is quite satisfactory, validating the accuracy of the SPH computations. Besides, the numerical wave celerity c is computed to be around 1.55–1.47 m/s under different immersion conditions. These values are also well consistent with the theoretical ones estimated by $c = \sqrt{\mathbf{g}(H + d)}$.
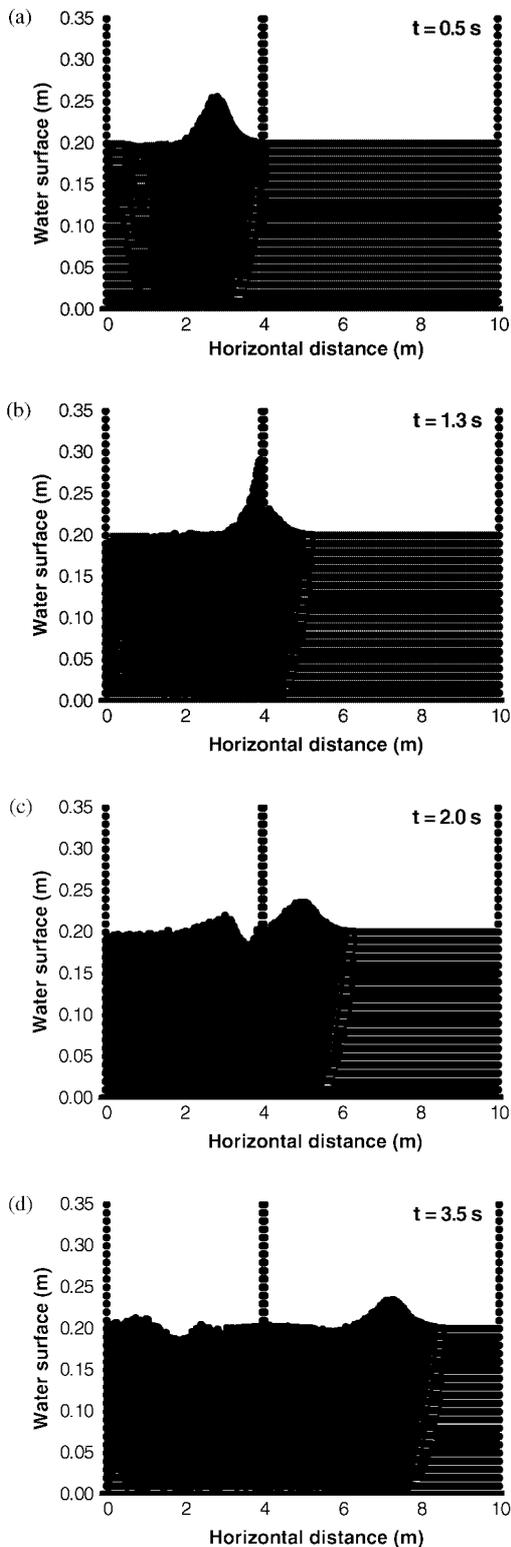
Figure 4   (a–d) Time series of solitary wave before and after impacting on curtain wall under immersion depth $d_{\mathrm{immer}}/d = 0.50$.

Figure 5   (a–d) Computational and theoretical transmitted solitary wave profiles under different immersion depths d_{immer}/d.

Wave energy dissipation is the main topic of interest in the study of breakwaters. During the solitary wave interacting with the curtain breakwater, a part of the incident wave energy is expected to dissipate due to the vortex shedding at the bottom tip of the barrier due to energy transmission, wave breaking and turbulence developed during the run-up and run-down processes. Apart from reflection, the partially immersed vertical barrier
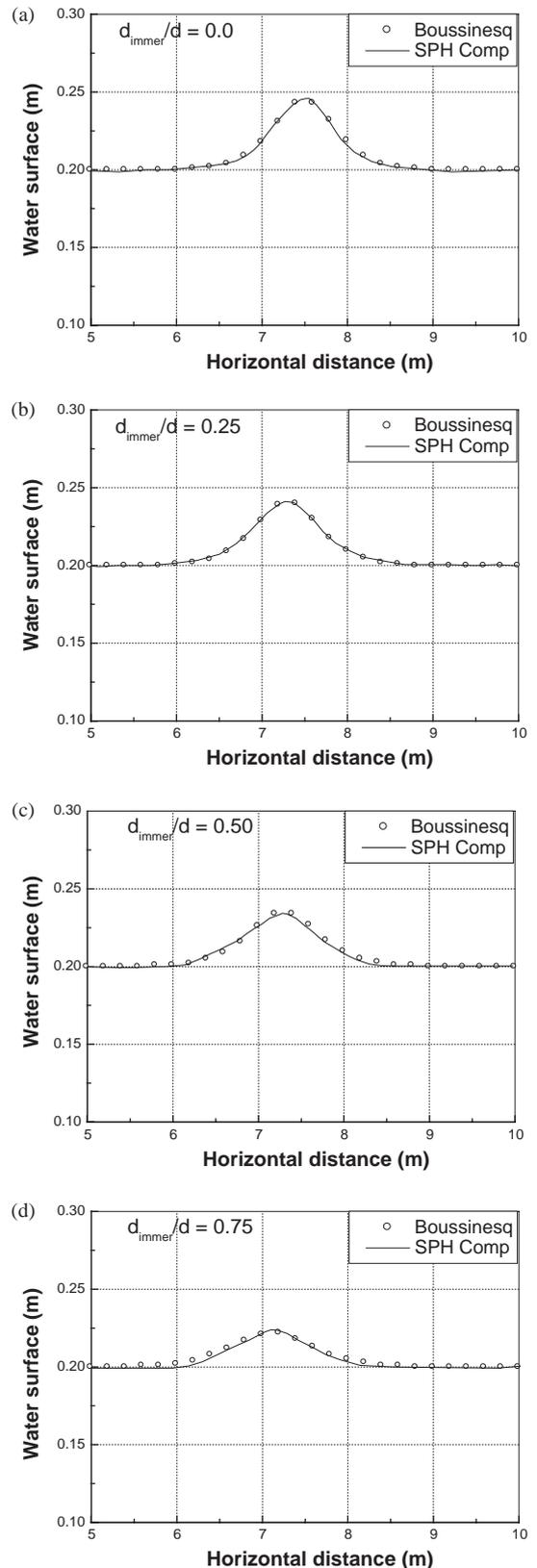
transmits the remaining part of wave energy from the incident wave. If we define the coefficient of transmission as $K_{\mathrm{t}} = H_{\mathrm{t}}/H_{\mathrm{i}}$, reflection $K_{\mathrm{r}} = H_{\mathrm{r}}/H_{\mathrm{i}}$ and dissipation $K_{\mathrm{d}} = H_{\mathrm{d}}/H_{\mathrm{i}}$, where H_{t}, H_{r}, H_{d} and H_{i} are the transmitted, reflected, dissipated and

incident wave heights, respectively,the following relationship can be established by employing energy conservation law

$$K_t^2 + K_r^2 + K_d^2 = 1 \qquad (20)$$

In Fig. 6(a), the transmission coefficient K_t is plotted against different immersion depths d_{immer}/d based on the above SPH computations. It is shown that over half of the incident wave energy could be transmitted while the immersion depth d_{immer}/d is less than 0.50. However, the curtain breakwater tends to be very effective in deterring solitary wave when its immersion depth is over 50%, from which point the coefficient of transmission begins to decrease rapidly until it attains a small value of 35% at $d_{immer}/d = 0.75$. This finding is also supported by the experimental results of Reddy and Neelamani (1992), who carried out a detailed study on regular wave dissipation by a partially immersed vertical barrier.

By employing the energy conservation Eq. (20), the calculated coefficient of dissipation K_d is plotted against different immersion depths d_{immer}/d in Fig. 6(b). It is interesting to see that K_d increases proportionally with the immersion depth at the beginning. However, it tends to be a constant value of 75% after the immersion depth reaches 50%. This phenomenon is due
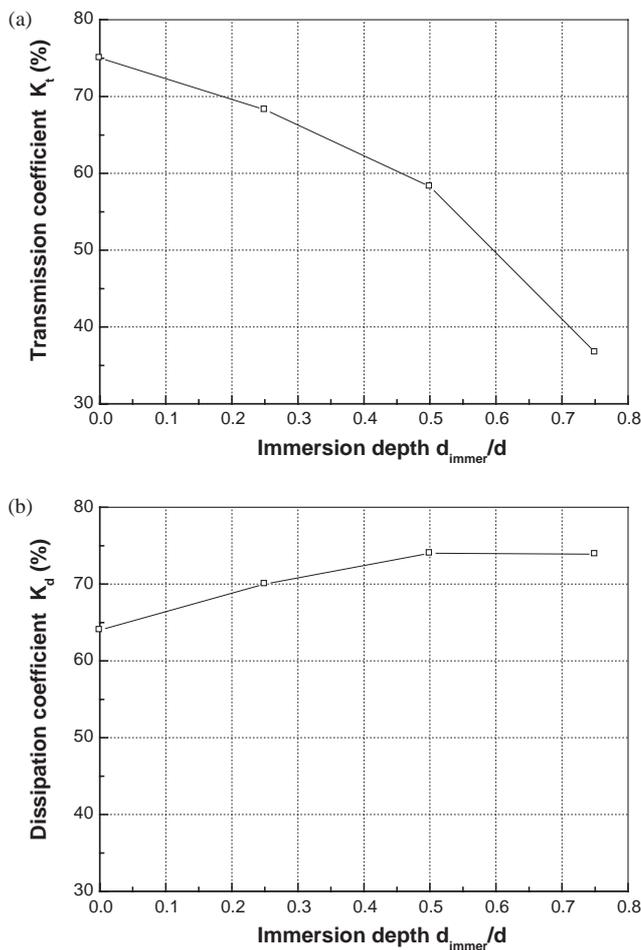
to the fact that the smaller transmission usually leads to larger reflection and the wave dissipation remains almost unchanged as a result. Besides, it is primarily found that the immersion depth $d_{immer}/d = 0.50$ is a critical parameter in evaluating the breakwater behavior under solitary wave conditions.

The prediction of hydrodynamic forces exerting on the curtain barrier is an important issue in the planning, design and monitoring of such breakwaters as a permanent structure with necessary depth of immersion. As wave interacts with the barrier, each side of the barrier experiences fluctuating pressures and, because these pressures differ on the up-wave and down-wave sides, the barrier also experiences time-varying wave forces. Based on SPH computations, the time sequences of wave forces on the curtain wall are shown in Fig. 7, under conditions of different immersion depths of $d_{immer}/d = 0.0, 0.25, 0.50$ and 0.75. The wave forces were obtained by integrating the computed pressure values on both sides of the curtain barrier and normalized by $\rho \mathbf{g} d^2$ in the figure. It is shown that all cases follow a similar evolution pattern, i.e., a sudden increase of net forces up to the peak followed by a rapid decay of their intensity to zero. The maximum forces occur during the maximum run-up on the curtain wall by the incident wave and the wave forces increase with the increasing immersion depth. It is quite consistent with the numerical results by Cooker *et al.* (1997) and Madsen *et al.* (2002) in that the maximum wave force occurs during the maximum run-up in case of smaller amplitude solitary waves. However, it is different from their computations in that shorter duration and smaller magnitude of the maximum forces are observed. This is because the transmission underneath the curtain wall greatly reduces the hydrodynamic force (by about 2/3 in the computation at $d_{immer}/d = 0.75$) as compared with a fully immersed case like that in Cooker *et al.* (1997) and Madsen *et al.* (2002). Fig. 7 also indicates that the hydrodynamic forces change rapidly from $d_{immer}/d = 0.50$ to 0.25, implying that $d_{immer}/d = 0.50$ is a key parameter, which is consistent with the conclusion drawn above from the analysis of wave energy.
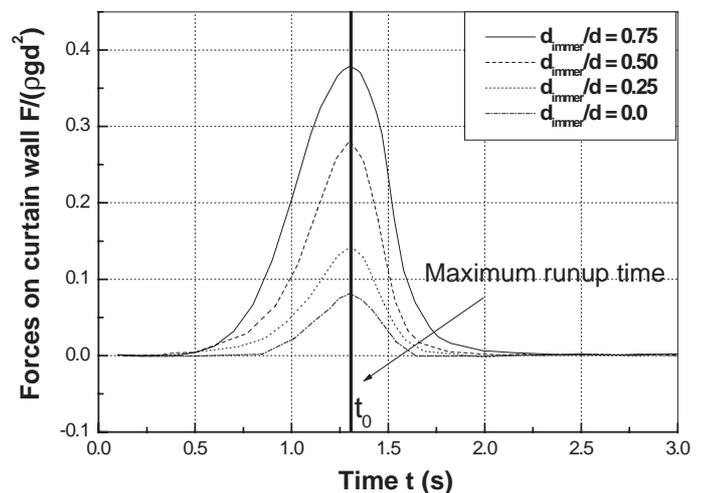

Figure 6 (a) Transmission coefficient K_t under different immersion depths d_{immer}/d. (b) Dissipation coefficient K_d under different immersion depths d_{immer}/d.

Figure 7 Time sequences of wave forces on curtain barrier under different immersion depths d_{immer}/d using smaller wave ($\varepsilon = 0.3$).

7.2 *Larger amplitude solitary wave ($\varepsilon = 0.6$) impacting on curtain wall with different immersion depths*

In this section we consider a larger amplitude solitary wave ($\varepsilon = 0.6$) interacting with a partially immersed curtain breakwater. According to SPH computations, the wave reflection, transmission and energy dissipation characteristics of the larger solitary wave are almost identical to those of the smaller solitary wave ($\varepsilon = 0.3$), which have already been shown in detail in the previous section. Thus they will not be further re-addressed in the paper.

However, the hydrodynamic force on the curtain wall by the larger amplitude solitary wave is totally different from that by the smaller solitary wave, in that it becomes double peaked for the higher wave. In Fig. 8, the time sequences of the normalized wave force under different immersion depths are shown. A double peaked wave force pattern is observed before and after the maximum run-up, which occurs at about time $t_0 = 1.2$ s. The magnitude of the second peak is slightly smaller as compared with the first one. These phenomena have already been justified by Cooker *et al.* (1997) and Madsen *et al.* (2002) in their computations of larger amplitude solitary waves interacting with a fully immersed curtain wall. However, the magnitude of the maximum force in our computation is only 1/3 as compared with their results. This is also attributed to the fact that the transmission underneath the curtain barrier greatly reduces the hydrodynamic forces. The mechanism behind this double force peak by the larger solitary wave is the mutual interaction between the hydrostatic and dynamic forces and can be easily understood in the following way: if we split up the total pressure into a hydrostatic part which is measured from the instantaneous position of the free surface and an acceleration part which includes non-linear velocity terms and the temporal derivative of the vertical velocity, it is very obvious that the hydrostatic part has only one maximum value, which occurs during the maximum run-up at time t_0. On the other hand, the dynamic part has two extremes just before and after the maximum run-up and thus increases the pressure above the hydrostatic level. Therefore, the two-peak force problem must

be carefully addressed during the practical design of breakwaters for defending against larger amplitude non-linear waves.

8   Conclusion

The paper presents an SPH particle model to simulate solitary wave reflection and transmission after impacting on a curtain-type breakwater. The model can easily and accurately track free surfaces by Lagrangian particles without numerical diffusion. The computations have been carried out under conditions of different immersions of the curtain wall using both smaller and larger amplitude non-linear waves. The computational results are in good agreement with those reported in the literature and show that the partially immersed curtain breakwater is effective in dissipating incoming wave energy if its immersion depth is over half of the water depth. Another important discovery is that the wave force on the curtain wall has only one single peak value in case of smaller waves while it has a double peak value in case of larger non-linear waves. This is caused by the counterbalance between the hydrostatic and dynamic forces during the wave run-up and run-down processes and should be paid great attention in practice for the purpose of breakwater safety.

Future improvement is needed to develop a better turbulence model to address the turbulence effect during wave breaking.

Notation

$$a = \text{Wave amplitude on constant water depth}$$
$$c = \text{Wave celerity} \ (=\sqrt{\mathbf{g}(d + H)})$$
$$d = \text{Constant water depth}$$
$$d_{\text{immer}} = \text{Immersion depth of curtain wall}$$
$$\mathbf{g} = \text{Gravitational acceleration}$$
$$h = \text{Kernel smoothing distance}$$
$$H_{\text{d}} = \text{Dissipated wave height}$$
$$H_{\text{i}} = \text{Incident wave height}$$
$$H_{\text{r}} = \text{Reflected wave height}$$
$$H_{\text{t}} = \text{Transmitted wave height}$$
$$K_{\text{d}} = \text{Coefficient of dissipation} \ (=H_{\text{d}}/H_{\text{i}})$$
$$K_{\text{r}} = \text{Coefficient of reflection} \ (=H_{\text{r}}/H_{\text{i}})$$
$$K_{\text{t}} = \text{Coefficient of transmission} \ (=H_{\text{t}}/H_{\text{i}})$$
$$l_0 = \text{Initial particle spacing}$$
$$m = \text{Particle mass}$$
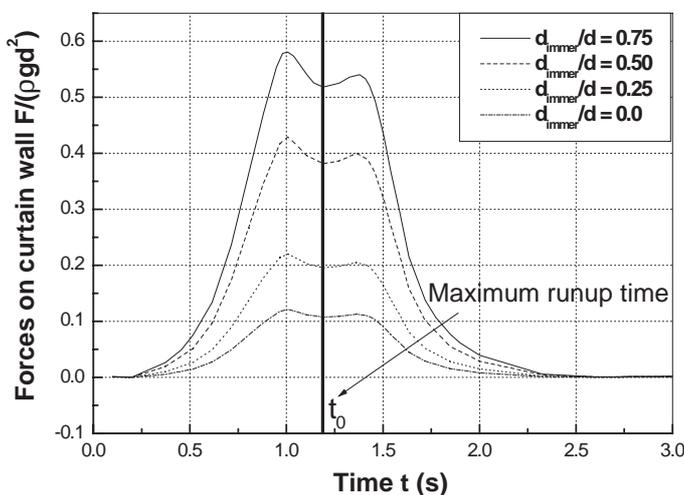$$N = \text{Number of particles}$$
$$P = \text{Pressure}$$

Figure 8   Time sequences of wave forces on curtain barrier under different immersion depths d_{immer}/d using larger wave ($\varepsilon = 0.6$)

q = Non-dimensional distance between particles $(=r/h)$
r = Distance between particles
$\mathbf{r}$ = Position vector
t = Time
t_0 = Time of maximum run-up
t_a = Time of attachment
t_d = Time of detachment
t_r = Wall residence time $(=t_d - t_a)$
$\mathbf{u}$ = Velocity
V_{max} = Maximum particle velocity
W = Interpolation kernel
Δt = Time increment
$\Delta\mathbf{u}$ = Changed velocity
ε = Non-linear wave parameter $(=a/d)$
η_0 = Maximum run-up elevation
η_a = Attachment elevation
η_d = Detachment elevation
ν_0 = Kinetic viscosity of laminar flow
ρ = Fluid density
ρ_0 = Initial density
τ = Time scale $(=\sqrt{d/\mathbf{g}})$
φ = Quantity interpolated/interpolating

Subscripts and symbols
a = Reference particle
b = Neighboring particles
ab = Value between particles a and b
$*$ = Intermediate value
$**$ = Corrected value

References

1. CHORIN, A.J. (1968). "Numerical Solution of the Navier–Stokes Equations". *Math. Comp.* 22, 745–762.

2. COOKER, M.J., WEIDMAN, P.D. and BALE, D.S. (1997). "Reflection of a High-Amplitude Solitary Wave at a Vertical Wall". *J. Fluid Mech.* 342, 141–158.

3. CUMMINS, S.J. and RUDMAN, M. (1999). "An SPH Projection Method". *J. Comp. Phys.* 152, 584–607.

4. DEAN, R.G. and DALRYMPLE, R.A. (1991). *Water Wave Mechanics for Engineers and Scientists*, Adv. Series Ocean Eng., Vol. 2. World Scientific, Singapore, pp. 295–325.

5. GOTOH, H. and SAKAI, T. (1999). "Lagrangian Simulation of Breaking Waves Using Particle Method". *Coast. Eng. J.* 41(3–4), 303–326.

6. HIRSCH, C. (1990). *Numerical Computation of Internal and External Flows*. Wiley, New York.

7. KOSHIZUKA, S., NOBE, A. and OKA, Y. (1998). "Numerical Analysis of Breaking Waves Using the Moving Particle Semi-Implicit Method". *Int. J. Numer. Methods Fluids* 26, 751–769.

8. KRIEBEL, D., SOLLITT, C. and GERKEN, W. (1998). "Wave Forces on a Vertical Wave Barrier". *Proc. 1998 26th Int. Conf. on Coast. Eng.*, ICCE-98, 22–26 June, Copenhagen, Denmark, pp. 2069–2081.

9. LEE, J.L. and LEE, K.J. (2001). "Wave Scattering by Multiple Permeable Barriers". *Int. Conf. on Port and Maritime R & D and Technology*, 29–31 October, Singapore, pp. 419–425.

10. LO, E.Y.M. (2000). "Performance of a Flexible Membrane Wave Barrier of a Finite Vertical Extent". *Coast. Eng. J.* 42(2), 237–251.

11. LOSADA, I.J., LOSADA, M.A. and BAQUERIZO, A. (1993). "An Analytical Method to Evaluate the Efficiency of Porous Screens as Wave Dampers". *Appl. Ocean Res.* 15, 207–215.

12. LUCY, L.B. (1977). "A Numerical Approach to the Testing of the Fission Hypothesis". *Astron. J.* 82(12), 1013–1024.

13. MADSEN, P.A., BINGHAM, H.B. and LIU, H. (2002). "A New Boussinesq Method for Fully Nonlinear Waves from Shallow to Deep Water". *J. Fluid Mech.* 462, 1–30.

14. MONAGHAN, J.J. and LATTANZIO, J.C. (1985). "A Refined Particle Method for Astrophysical Problems". *Astron. Astrophys.* 149, 135–143.

15. MONAGHAN, J.J. (1992). "Smoothed Particle Hydrodynamics". *Annu. Rev. Astron. Astrophys.* 30, 543–574.

16. MONAGHAN, J.J. and KOS, A. (1999). "Solitary Waves on a Cretan Beach". *J. Waterway Port Coast. Ocean Eng. ASCE* 125(3), 145–154.

17. NEELAMANI, S. and VEDAGIRI, M. (2002). "Wave Interaction with Partially Immersed Twin Vertical Barriers". *Ocean Eng.* 29, 215–238.

18. REDDY, M.S. and NEELAMANI, S. (1992). "Wave Transmission and Reflection Characteristics of a Partially Immersed Rigid Vertical Barrier". *Ocean Eng.* 19(3), 313–325.

19. SHAO, S.D. and LO, E.Y.M. (2003). "Incompressible SPH Method for Simulating Newtonian and Non-Newtonian Flows with a Free Surface". *Adv. Water Resour.* 26(7), 787–800.

20. TANAKA, M. (1986). "The Stability of Solitary Waves". *Phys. Fluids* 29, 650–655.

21. URSELL, F. (1947). "The Effect of a Fixed Vertical Barrier in Surface Waves in Deep Water". *Proc. Camb. Phil. Soc.* 43(3), 374–382.

22. WIEGEL, R.L. (1960). "Transmission of Wave Past a Rigid Vertical Thin Barrier". *J. Waterway Harbors Div., ASCE* 86(WW1), 1–12.